ELSEVIER

Astroparticle Physics 17 (2002) 279–292

Astroparticle Physics

www.elsevier.com/locate/astropart

Sensitivity of an underwater acoustic array to ultra-high energy neutrinos

Nikolai G. Lehtinen [a], Shaffique Adam [a,1], Giorgio Gratta [a,*], Thomas K. Berger [b], Michael J. Buckingham [b]

[a] *Department of Physics, Stanford University, Stanford, CA 94305-4060, USA*
[b] *Scripps Institution of Oceanography, UC San Diego, La Jolla, CA 92093-0238, USA*

Received 2 April 2001; accepted 13 July 2001

Abstract

We investigate the possibility of searching for ultra high energy neutrinos in cosmic rays using acoustic techniques in ocean water. The type of information provided by the acoustic detection is complementary to that of other techniques, and the filtering effect of the atmosphere, imposed by the fact that detection only happens if a shower fully develops in water, would provide a clear neutrino identification. We find that it may be possible to implement this technique with very limited resources using existing high frequency underwater hydrophone arrays. We review the expected acoustic signals produced by neutrino-induced showers in water and develop an optimal filtering algorithm able to suppress statistical noise. The algorithm found is computationally appropriate to be used as a trigger for the signal processors available on existing arrays. We estimate the noise rates for a trigger system on a very large size hydrophone array of the US Navy and find that, while a higher density of hydrophones would be desirable, the existing system may already provide useful data. © 2002 Elsevier Science B.V. All rights reserved.

PACS: 95.85.Ry; 13.85.Tp; 96.40.Tv; 96.40.−z

1. Introduction

The understanding of the highest energy cosmic rays represents one of the most challenging fields of modern physics. While abundant high quality data has greatly enhanced our knowledge of cosmic rays of energies up to several tens of GeV, the study of higher energies is limited by the low fluxes available. Yet the study of particles with energies in excess of 10^{18} eV (ultra-high energy cosmic rays, or UHECR) promises boundless opportunities of discovery. To date some 12 cosmic ray events have been observed with energy in excess of 10^{20} eV [1]. While the acceleration mechanisms at these energies are not completely understood [2], even more fundamental problems arise from the apparent inconsistency of data with the Greisen–Zatsepin–Kuzmin (GZK) cutoff. Such cutoff [3,4] is expected to limit the maximum energy of protons of cosmological origin somewhere below 10^{20} eV, because of the finite (≈50 Mpc) inelastic collision

* Corresponding author. Tel.: +1-650-725-6509; fax: +1-650-725-6544.
E-mail address: gratta@hep.stanford.edu (G. Gratta).
[1] Now at Cornell University.

0927-6505/02/$ - see front matter © 2002 Elsevier Science B.V. All rights reserved.
PII: S0927-6505(01)00158-X

length of such particles in the cosmic microwave background radiation (CMBR). Indeed the inelastic scattering of UHE protons off CMBR should at the same time suppress the proton flux and breed neutrinos from decay products of pions. While the present data seem to indicate that photons and neutrinos are not the main component of UHECR [1], reliable identification of the primary particle type and its energy are essential parameters for the study of this problem.

It was recently pointed out [5] that a substantial UHE neutrino component may accompany UHE protons and nuclei, due to neutrino production in cosmic beam dumps. Neutrino production at ultra-high energies appears in fireball models of gamma-ray bursts [6–8], active galactic nuclei [9–14] and, to a lesser degree, in Galactic mechanisms [15] and, as mentioned, the GZK process [16]. Another hypothetical source is the decay of heavy objects predicted by some theories, known as the "top–down" models of UHECR production [2, 17,18].

Weakly interacting neutrinos could, unlike UHE gamma rays and protons, reach us from distant and powerful sources, opening a deeper horizon for astrophysics, cosmology and, possibly, high-energy particle physics [9,19]. While atmospheric neutrinos represent an irreducible background for earth-based detectors, such a background is expected to be modest because of the extremely long decay length of pions at the energies of interest.

Three techniques have been used until now to detect UHECR, all involving the showering of the primary particle in the earth's atmosphere. The shower is then detected either by observing the fluorescence or Čerenkov light induced by the ionizing tracks in the air, or by directly detecting the charged particles in the shower tail with scintillation counters scattered on the ground [1,20, 21]. While some of the these techniques provide the largest acceptances obtained in particle detectors, in general the study of UHECR is still hampered by the very low flux one has to be sensitive to. Typical fluxes are $\sim$100 km^{-2} year^{-1} above 10^{18} eV, $\sim$1 km^{-2} year^{-1} above 10^{19} eV, and $\sim$1 km^{-2} century^{-1} above 10^{20} eV [1]. Dedicated neutrino telescopes using Čerenkov light under water and the Antarctic ice cap are for the time being optimized for the TeV–EeV energy region [5].

While much has been learned from the above detectors, it is important to explore, in parallel, new methods that could either increase the flux sensitivity, and hence raise the energy threshold for detection, or help constraining the primary particle identification and its energy. Alternative methods being discussed [9] include the detection of radio Čerenkov emission from the lunar soil [22] (sensitive only to neutrinos that can cross the moon and interact upon exiting the satellite from its near side) and active radar detection of showers in the atmosphere [23] (which has different systematics for particle identification since it is more sensitive to horizontal showers than other techniques). As discussed in this paper, another possibility consists in the detection of showers by means of the acoustic energy released in the medium where they develop. While, at least in principle, this technique could use as a radiator either the soil of the moon or a large body of water on the earth, here we concentrate on the second case that is more practical and, as we will show, may be possible to test on a large scale with a very modest effort. It is important to realize that these two radiators would provide very different information, the first being sensitive to UHECR of any type, while the second being sensitive essentially only to neutrinos because of the filtering effect of the earth's atmosphere. While the idea of taking advantage of the very high mechanical Q for small oscillation amplitudes and ultra-low seismic noise characteristic of the moon was first mentioned in Ref. [24], acoustic detection of ionizing particles in water was proposed in Ref. [25] and then developed [26] in connection with the DUMAND project [27–29]. Although the primary goal of DUMAND was optical Čerenkov detection of muon tracks in deep ocean water, the hydrophones, originally conceived to monitor photomultiplier positions, were proposed to be used for acoustic detection of neutrinos of $>10^{16}$ eV energy. These early ideas were nicely complemented by experimental data collected at accelerators [30]. We will review the past work on the subject and present a model useful to study UHE neutrino detection in sea water. We will then use this model to simulate signals and develop an algorithm to optimally filter

hydrophone data to extract the expected signals from statistical noise. While most of the assumptions in our study are rather general, we will apply our results to the case of a large, high frequency test array that the US Navy operates off the coast of Florida.

We note here that UHE neutrino fluxes substantially larger than the UHECR flux quoted by the experiments utilizing air showers could have gone unobserved. The neutrino cross-section due to neutral and charged current interactions in the UHE regime is calculated in Ref. [31]. Even for $E_\nu \sim 10^{20}$ eV the probability of interaction in traversing entire atmosphere's depth is only of the order of 10^{-5}. Many models [8,10–14,17,18], predict neutrino fluxes higher than the flux of the UHECR observed in the atmosphere. For example, fireball gamma-ray burst models predict a neutrino flux at energies $E_\nu > 10^{20}$ eV as high as ~ 1 km^{-2} year^{-1}, active galactic nucleus models ~ 0.1 km^{-2} year^{-1}, and top-down models ~ 10 km^{-2} year^{-1}, as quoted in Ref. [31].

2. Acoustic signature of particles in water

At the energies of interest here, neutrinos interact in water by a deep inelastic scattering on quarks inside oxygen and hydrogen nuclei. The scattering produces a lepton and an hadronic shower, with similar energies shared among these two components. The structure of hadronic showers is the same for all three flavors of (anti)neutrino. The behavior of the leptons, however, is different. In the case of ν_e the lepton energy goes in an electromagnetic shower and is essentially detected together with the hadronic energy. For ν_μ calculations by Mitsui [34] show that the mean-free-path in water between catastrophic bremsstrahlung and direct pair production events with energy transfer greater than 10^{19} eV is large (several km) with respect to the vertical size of the detectors considered here. The residual ionization along the track is low, so that muons are virtually undetectable by acoustic methods [28]. Tau neutrinos create τ leptons, whose mean free path turns out to be long enough to leave the detector volume for $E_{\nu_\tau} \gtrsim 10^{17}$ eV.

At $E_\nu \sim 10^{20}$ eV in water a hadronic shower deposits 90% of its energy in a cylinder of some 20 cm radius and 20 m length. Sound is produced in water mainly by heating localized along the shower, resulting in volume expansion, as first suggested in Ref. [25]. The shower development (and hence the energy deposition) occurs at the velocity of light and can be regarded as instantaneous for the purpose of acoustic phenomena. As already mentioned the sound generation has been confirmed experimentally using artificial particles [30]. Although it is not completely clear to what extent these accelerator experiments, simulating $\sim 10^{20}$ eV energies using bunches of over 10^{11} protons of ~ 200 MeV, can describe the details of the lower energy-density UHE neutrino interactions, their accuracy is probably sufficient for the present study.

We analyze the acoustic signal production following Ref. [26]. Let the energy deposited per unit volume per unit time be given by a function $E(\mathbf{r}, t)$. The total neutrino energy is $E_0 = \int_V E(\mathbf{r}, t) \mathrm{d}^3\mathbf{r}$. The wave equation for the pressure pulse produced p is:

$$\nabla^2 \left(p + \frac{1}{\omega_0} \dot{p} \right) - \frac{1}{c^2} \ddot{p} = - \frac{\beta}{C_p} \frac{\partial E}{\partial t}, \tag{1}$$

where we use the parameters for sea water: $c \approx 1500$ m/s is the speed of sound, $\beta \approx 1.2 \times 10^{-3}$ K^{-1} is the bulk coefficient of thermal expansion, $C_p \approx 3.8 \times 10^3$ J kg^{-1} K^{-1} is the specific heat at constant pressure, and $\omega_0 \approx 2.5 \times 10^{10}$ s^{-1} is the characteristic attenuation frequency. ω_0 is, strictly speaking, a function of frequency [32], as can be seen from the plot of the attenuation coefficient α (dB/km) $= (10^4 / \ln 10 \omega_0 c)(2\pi f)^2$ in Fig. 1. For simplicity of calculations, we assume that ω_0 is a constant in the frequency range $f = 10$–100 kHz characteristic of the signal.

We note here that the coefficient of thermal expansion β depends upon the water temperature. It vanishes at ~ -3 °C for typical sea water of 3.5% salinity [35]. In the case of vanishing β other mechanisms of energy coupling to acoustic modes have been proposed [36,37]. Extreme temperature profiles as a function of depth are given in Fig. 2 for the tropical waters of the site discussed below.

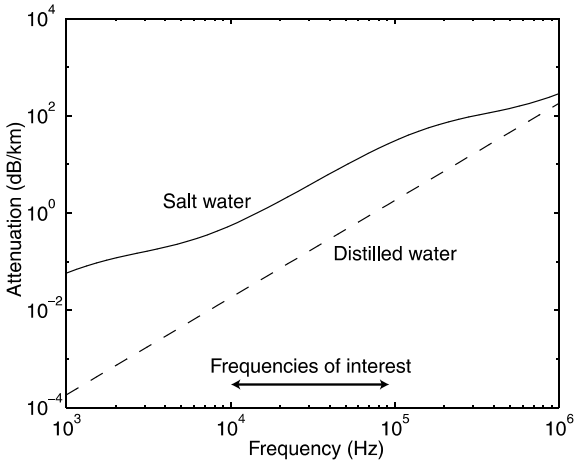

Fig. 1. Sound attenuation coefficient at 25 °C, in the sea and distilled water as function of frequency [32].

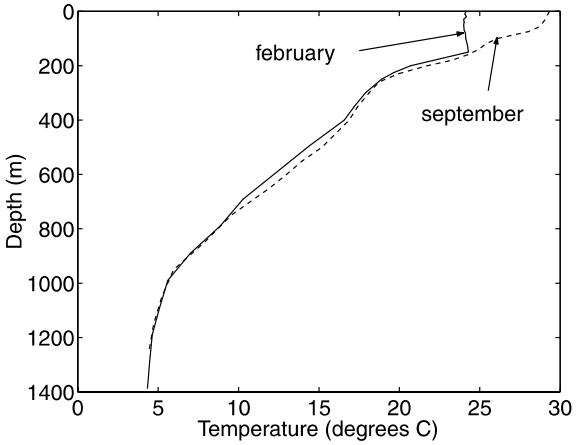

Fig. 2. Water temperature profiles for the tropical region of the AUTEC array discussed below [33]. The two curves correspond to the extreme variations of temperature through the year.

As we can see, although β decreases with depth, it does not reach zero, so we will restrict ourselves to the case of thermal emission mechanism.

The instantaneous nature of the heating mechanism can be expressed by $E(\mathbf{r}',t) = E(\mathbf{r}')\delta(t)$. The pressure wave can then be calculated at location $\mathbf{r}$ as a function of time t as

$$p(\mathbf{r},t) = \int_V E(\mathbf{r}')G(\mathbf{r}-\mathbf{r}',t)\,\mathrm{d}^3\mathbf{r}',$$

where $G(\mathbf{r},t)$ is the pressure pulse generated by a point source $E = \delta(\mathbf{r})\,\delta(t)$, taking attenuation into account:

$$G(\mathbf{r},t) = -\frac{\beta}{4\pi C_p}\,\frac{(t-r/c)}{r\sqrt{2\pi}\tau^3}\,\exp(-(t-r/c)^2/(2\tau^2)), \tag{2}$$

where $\tau = \sqrt{r/(\omega_0 c)}$.

The region of energy deposition is elongated in the direction of the initial velocity of the neutrino, which constitutes the axis of the cascade. The acoustic emission is coherent in the plane perpendicular to this axis. Thus, the radiation diagram has a pancake shape, perpendicular to the shower axis, as shown in Fig. 3. This effect was also observed in the 30 cm long and 4.5 cm wide cylinder energy deposition by particles in one of the accelerator experiments described in Ref. [30].

We calculate the time dependence of the pressure at a distance $r = 1$ km from the origin, for different directions of observation. As shown in Fig. 3, the angle θ is calculated in the forward direction from the perpendicular to the shower axis and the origin is at the starting point of the shower. Since the maximum energy deposition does not occur at the beginning of the shower, the maximum acoustic pulse results at some angle $\theta > 0$.

To calculate the effect of a 10^{20} eV hadronic shower, we use a model based on the results of one-dimensional Monte Carlo simulations in ice [38]. This model includes the interactions of π^0 and other short-lived resonances, as well as the Landau–Pomeranchuk–Migdal (LPM) effect [39–42], that are important at UHE. The transverse structure is modeled after Ref. [43]. The results of acoustic emission by a hadronic shower are presented in Fig. 4.

The pressure pulse has a typical bipolar shape and is shown, at the maximum of the radiation pattern, in Fig. 4a. The peak pressure and energy fluence for other angles of observation are shown in Fig. 4b. The signal at other observation angles has a smaller amplitude and is stretched in time, still preserving the bipolar shape.

To calculate the case of an electromagnetic shower we use the Monte Carlo model LPM-SHOWER [44] that includes the LPM effect. In

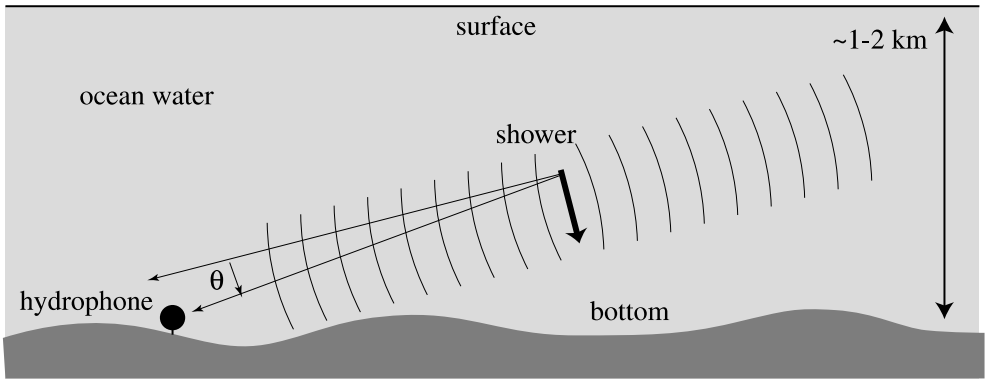

Fig. 3. Geometrical configuration of a shower and acoustic pulse produced. The angle θ is calculated with respect to the forward direction from the perpendicular to the shower axis. The origin is at the starting point of the shower.

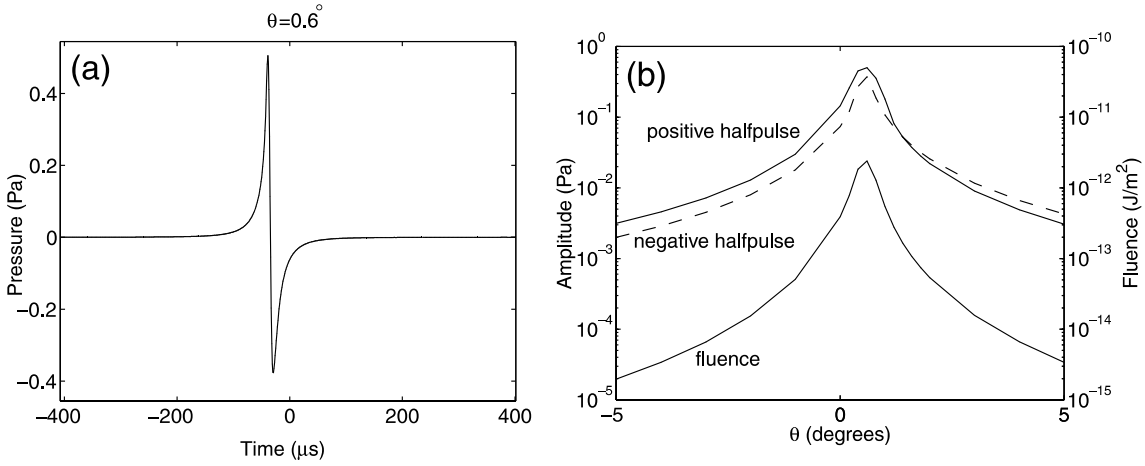

Fig. 4. Results of calculations of the acoustic signal from the hadronic part of the neutrino-induced shower [38], at the distance of 1000 m from the shower axis, for a primary hadronic energy of 10^{20} eV: (a) the pulse shape at the observation angle of $\theta = 0.6°$, where the amplitude is maximal, (b) the pressure amplitude of the pulse and the total energy fluence in the pulse, $(\rho c)^{-1}\int_{-\infty}^{+\infty} p^2\,\mathrm{d}t$. These last two quantities are plotted as functions of observation angle as defined in Fig. 3.

this case, with all the energy in the electromagnetic channel, the LPM effect dominates the shower shape, resulting in very large fluctuations, and a significant elongation for initial energies $\gtrsim 1$ EeV. For $E_e = 10^{20}$ eV the shower is $\sim$300 m long. The non-uniform energy deposition is the result of individual sub-showers starting at the locations of large energy loss. These sub-showers also create peaks in the acoustical radiation pattern. The properties of a typical shower are presented in Fig. 5. The multi-peak structure is clearly visible in the amplitude and fluence diagrams as a function of the angle. While the pressure pulse shape, taken at the direction of maximum emission, has, also in this case, a simple bipolar shape, the maximum occurs at a large angle respect to the previous case, because of the longer shower profile.

The signal from electron (anti)neutrinos is the superposition of these two cases in a proportion corresponding to the way the energy of the primary is shared between the hadronic and electromagnetic shower. It was found [19] that at $E_{\nu(\bar{\nu})} = 10^{20}$ eV the hadronic component accounts for $\sim$20% of the total energy. For an UHE primary,

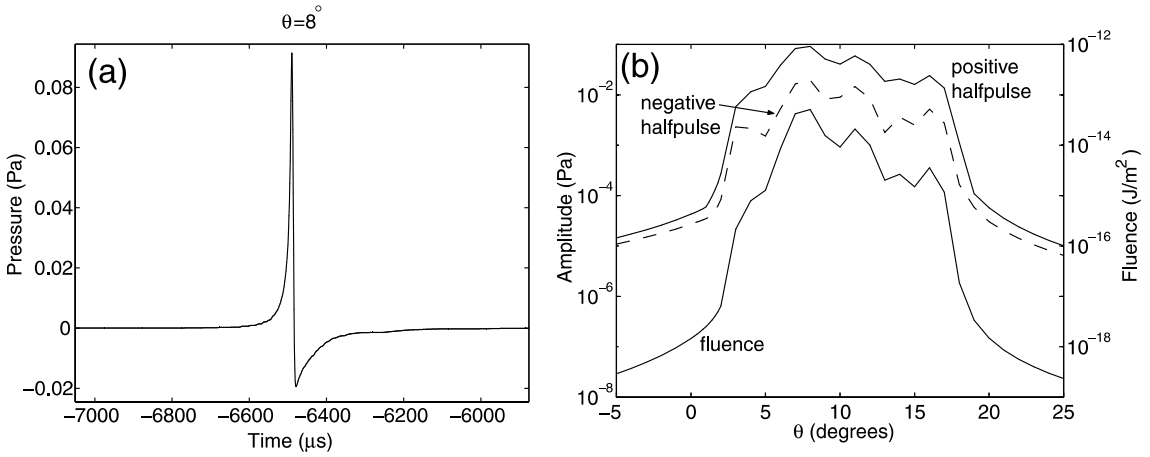

Fig. 5. The results of calculation of the acoustic signal from the electromagnetic part of a $\nu_e(\bar{\nu}_e)$-induced shower [38,44], at the distance of 1000 m from the shower axis. The total energy in the electromagnetic shower is 10^{20} eV. (a) The pulse shape at the observation angle of $\theta = 8°$, where the amplitude is maximal, (b) the amplitude of the pulse and the total energy fluence in the acoustic pulse, $(\rho c)^{-1}\int_{-\infty}^{+\infty} p^2\,dt$. Both are plotted as functions of observation angle as defined in Fig. 3.

the axes of the hadronic and electromagnetic showers are practically parallel, the angle between them being of the order of 10^{-6} radians [34].

We note here that the peak pressures predicted at 1000 m from 10^{20} eV showers are well within the sensitivity of good quality hydrophones. Indeed typical sensitivities for the frequency band of interest are $\sim 10^{-3}$ Pa [30]. However it is rather clear that the two factors limiting the power of this technique will be the ambient noise and the characteristic emission pattern described above. Such pattern substantially limits the solid angle accessible to each sensor and hence, together with the noise level, it will dictate the maximum tolerable spacing between detection sites.

3. The AUTEC array as a UHE neutrino detector

While the installation of hydrophones to complement underwater Čerenkov arrays has been discussed by several groups [45,46], it is interesting to consider whether a very large existing array could be used in parasitic mode for UHE neutrino detection. Although the scientific community has recently started discussing the use of long-range, early warning military arrays for a variety of oceanographic purposes [47], the low bandwidth of these systems, essentially designed to detect low-frequency ship noise that can propagate over very large distances, make them quite unsuitable for the type of signals discussed here. Another type of array exists, generally designed to track ships and weapons equipped with special high frequency "pingers" during limited range naval exercises. Such arrays have a relatively high-density of hydrophones with typical bandwidths in the tens of kHz. The array considered here, at the Sites 3 and 4 of the Atlantic Undersea Test and Evaluation Center of the US Navy (AUTEC) [48], covers an approximate area of 250 km^2 ($\approx 5 \times 15$ nautical miles^2) with depths between 1400 and 1600 m, as shown in Fig. 6.

AUTEC is located in the "Tongue of the Ocean", a 50×200 km^2 tract of deep sea, bounded to the west by Andros Island and to the south and east by large areas of very shallow banks in the Bahamas. This peculiar geographical configuration, with shipping access only from the north through the narrow Providence Channel, provides quiet conditions, because of the low boat traffic and sluggish currents.

Individual hydrophones at Sites 3 and 4 are mounted at the ends of 4.5 m long booms extending above the ocean floor. A total of 52 sensors cover the two sites, arranged on a triangular

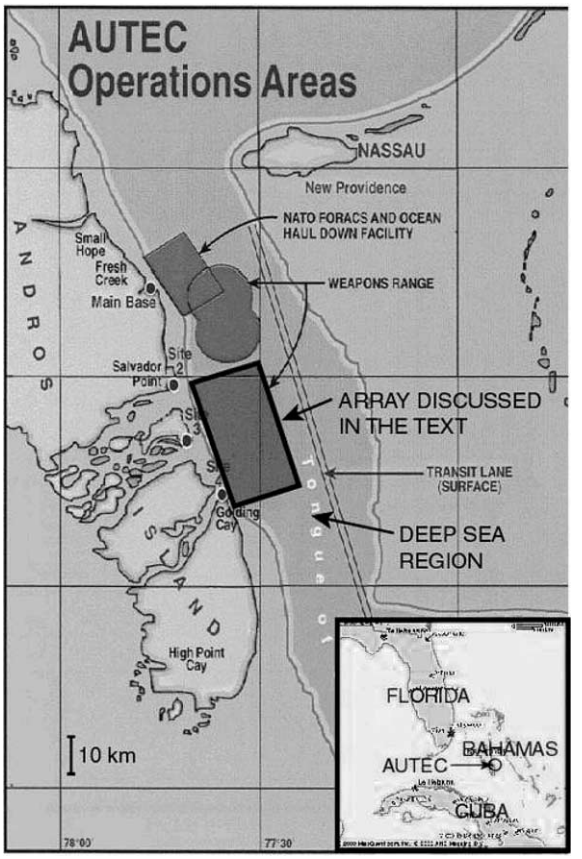

Fig. 6. Schematic view of the AUTEC facilities. The hydrophone array discussed in the text is the larger quadrangular region.

lattice with ≈2.5 km sides. Analog signals from each hydrophone are preamplified and brought to shore where digitizers and processors are located. The frequency response of the hydrophone and analog chain is flat to within ±5 dB in the range from 1 to 50 kHz, while the sampling rate of the digitizers is about 100 kHz. Accurate GPS time stamping is provided in the data stream. In its normal operation the system is capable gathering highly accurate three-dimensional in-water tracking data. While a denser sensor spacing would of course be desirable, the shower-to-hydrophone distance of 1 km we use though this work is close to the worst case scenario of a neutrino interacting half-way between two sensors.

In Fig. 7 we show the random noise levels at AUTEC for different wind conditions, along with

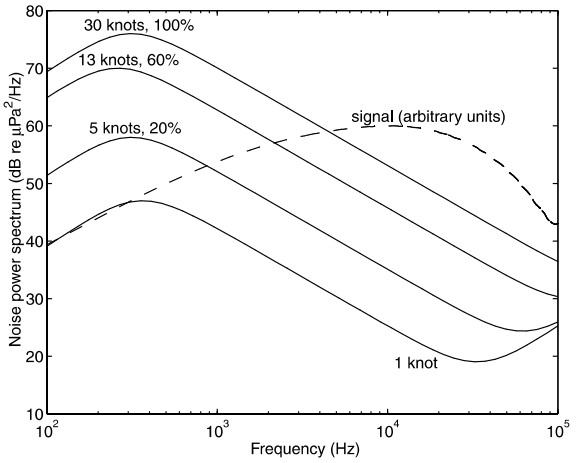

Fig. 7. Ambient noise spectra at AUTEC for different wind speeds in knots (1 knot = 0.5144 m/s) and the approximate spectrum of the expected neutrino signal. The absolute amplitude of the signal is, of course, dependent upon the energy of the primary and the location of the impact relative to the hydrophone. The percent figure given next to each noise curve represents the cumulative probability of finding such (or better) conditions at a given time.

the cumulative probability for such conditions to occur on range. The approximate frequency spectrum of the expected neutrino signals is also given for reference. The noise spectra in Fig. 7 are due to the waves at the ocean surface induced by wind [49–51] and, above $\gtrsim 10$ kHz, to thermal noise [49]. In addition coherent noise from human activities and natural phenomena should be considered. A-priori we expect two types of artificial noise: the first, due to ship screws, is mainly confined to low frequency and hence easy to reject, while the second, due to the range ''pingers'', is concentrated at a few well known frequencies and, again, easy to filter out. In general exercises are performed on range roughly 50% of the time, so that very little man-made noise is expected for a substantial fraction of every day (typically outside of working hours). More serious is probably the high frequency noise produced by marine mammals using sonar to localize their prey and snapping shrimps [52]. The severity of these backgrounds depends on the season and can only be quantitatively understood by analyzing a substantial amount of data from the array. Here we limit ourselves to a detailed analysis of the random

noise, formulating a filtering algorithm that can be implemented on the digital signal processors (DSP) that analyze on-line the time-series from each hydrophone. This system of data selection can be used essentially as a trigger signal to log an interval of the data stream for the entire array (or maybe only some subset of sensors near to the one producing the trigger). Further data reduction, possibly involving the correlation of signals from different sensors, can then be done off-line.

Scattering of sound off the ocean surface and bottom may alter somewhat the simple picture given above. For instance we expect that each hydrophone will generally record two pulses: the direct one and the one scattered from the ocean floor immediately around the sensor. The time delay will be of the order of $h/c \sim 3$ ms, where $h = 4.5$ m is the height of the hydrophones above the bottom. This effect can be used to estimate the angle of incidence of the acoustic wave and hence of the shower axis. In addition scattering phenomena can make the event detectable by more than one hydrophone. The attenuation and re-emission patterns from scattering at the sea-bed and surface (where bubbles play an important role) can be numerically estimated [53,54]. While large attenuations are to be expected so that it appears unlikely that these phenomena can be used to trigger an event that for geometrical reasons was not directly visible, it is probable that scattered signals can be detected below threshold by sensors in the vicinity of the triggering hydrophone. While off-line study of these correlations would be particularly important in confirming the event and in measuring position, orientation and energy of the shower, in the rest of this paper we concentrate on the triggering function that has to rely on single sensors.

4. Random noise and single-sensor sensitivity

In order to analyze the problem of signal detection in some detail we assume a discrete data sample set x_k $(k = 0, \ldots, M-1)$ with a sampling rate of $f_s = 100$ kHz, as provided by the AUTEC digitizers. We consider the detection from a single site, as it is natural given the small probability that the radiation pattern discussed in the previous section would intercept more than one hydrophone. Sub-threshold use of signals from neighboring hydrophones may be possible in off-line analysis but it is not discussed here. The data are the sum of the stationary Gaussian noise of a given power spectrum and a signal of a given shape, but unknown amplitude, starting at position k_0 in the data set, as illustrated in the simulated time series of length $M = 10\,000$ in Fig. 8. In this Figure a signal from a 2×10^{19} eV hadronic shower at 1 km with the optimal angular orientation to illuminate a hydrophone has been superimposed at a random time (chosen in this case to start at sample number $k_0 = 5000$) over the statistical noise spectrum relative to 13 knots wind from Fig. 7. These conditions (or better) occur at the AUTEC site 60% of the time. The sampling frequency is high enough to provide negligible distortions.

We extract the signal using the algorithm described in Appendix A, which is based on the digital filter of transfer function H_l calculated on the basis of the signal shape and the Gaussian noise spectrum given in Eq. (A.4). The variable Y_k resulting from the application of the filter

$$Y_k = \sum_{l=k}^{k+N-1} H_l x_{k+l}$$

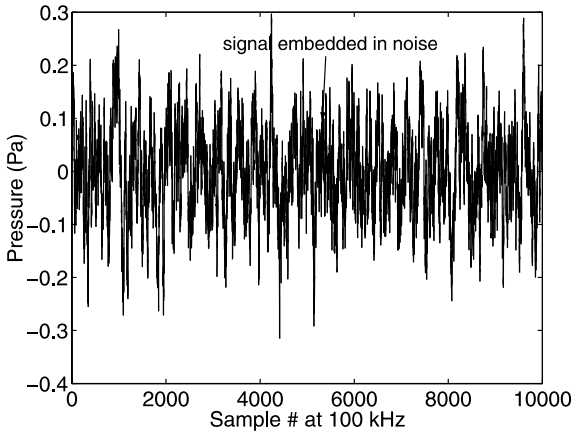

Fig. 8. The signal from 2×10^{19} eV hadronic shower artificially embedded in the noise sample of length $M = 10\,000$ at position $k_0 = 5000$. The noise is simulated using the spectrum for wind speed of 13 knots. The time interval of this sample is 0.1 s.

has a Gaussian distribution and is used to assert the presence of the signal, using a threshold $Y_{\rm th}$ that can be chosen for a certain detection efficiency and false-alarm rate at a given signal amplitude A ($Y_k > Y_{\rm th}$ indicating the presence of a signal). In practice the value of N can be made small enough for efficient calculation on the commercial DSP processors used at AUTEC.

In Fig. 9 we plot the variable Y_k for the time series in Fig. 8. We see that Y_k at the time sample $k = k_0 = 5000$ has a value substantially higher than elsewhere. Using a threshold $Y_{\rm th} = Y_{k_0}$, we find the probability of false alarm to be 5×10^{-16} at each data point. On the other hand the naive technique of trying to find the signal using an amplitude threshold in the time domain would give a false alarm probability of 0.14 at each sample point, with a threshold set at the amplitude of the signal. The effectiveness of the method, also evident by simple inspection of Figs. 8 and 9, is based on the difference between the signal and noise spectra in Fig. 7. This technique is equivalent to the application of a matched filter [27,55]. A value of $N = 7$ was used in the calculation, giving $\sim$15 floating-point operations at each data point, which corresponds to a processor speed requirement of 1.5 Mflop/s. The duration and amplitude of the signal can be estimated by maximizing a likelihood function.

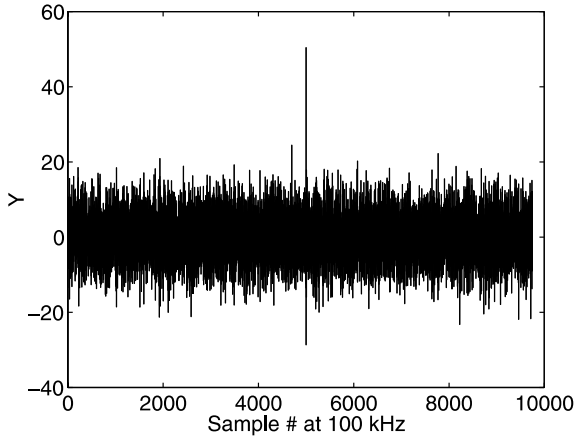

Fig. 9. The variable Y discussed in the text and computed in detail in Appendix A (see Eq. (A.3)) for the time series shown in Fig. 8. A prominent peak at the correct location of $k_0 = 5000$ is clearly visible.

We now use the probabilities of a signal miss and a false alarm found in Appendix A to quantitatively analyze the power of the array as a UHE neutrino detector. Here we stress the fact that our analysis does not take into account possible interference from coherent sources, as already mentioned above.

We define the detector efficiency as the fraction of neutrinos that are detected with respect to those interacting in the volume of water $\varepsilon = \Lambda/\Lambda_0$. We can write the interaction rate Λ_0 as

$$\Lambda_0 = F(E) N_A \rho_{\rm w} \sigma(E) V_{\rm w},$$

where $F(E)$ is the UHE neutrino flux at energy E, $\sigma(E)$ is the cross-section of interaction with a nucleon, $N_A\rho_{\rm w}$ is the number of nucleons in unit volume of water, and $V_{\rm w} = ah$ is the volume of the detector (a and h being the area and average depth of the array). The detected rate is limited by the effective volume of the radiation pattern $V_{\rm E}$ in which the amplitude of the signal (relative to produced by a shower of energy 10^{20} eV at a distance of 1 km) is above the detection threshold A. We can write $V_{\rm E}$ as:

$$\left(\frac{V_{\rm E}}{1\ {\rm km}^3}\right) = \frac{2\pi\Delta\theta}{3}\left(\frac{R_{\rm E}}{1\ {\rm km}}\right)^3 = \frac{2\pi\Delta\theta}{3}\left[\left(\frac{E}{10^{20}\ {\rm eV}}\right)\frac{1}{A}\right]^3, \quad (3)$$

where $\Delta\theta$ is the effective angular extent of the radiation lobe that can be found by integrating the curves in Figs. 4b and 5b, and $R_{\rm E}$ is its radial extent. We obtain $\Delta\theta \simeq 0.5°$ ($\Delta\theta \simeq 1.5°$) for showers induced by ν_μ, $\bar{\nu}_\mu$, ν_τ, $\bar{\nu}_\tau$ ($\nu_{\rm e}, \bar{\nu}_{\rm e}$). The difference comes about from the electron neutrinos having the electromagnetic part of the shower, while other flavors have only hadronic part. We note that the expression for $V_{\rm E}$ includes a signal amplitude inversely proportional to the distance R_0, as it should in our regime of radiation [26].

The rate of detected neutrinos is then found by integrating over volume:

$$\Lambda = N_{\rm h} F(E) N_A \rho_{\rm w} \sigma(E) \int_0^{V_{\rm E,max}} p_{\rm detect}(A, Y_{\rm th})\, {\rm d}V_{\rm E}, \quad (4)$$

where $N_{\rm h}$ is the number of hydrophones and $p_{\rm detect}$ is the detection probability given in Eq. (A.7), with A found from $V_{\rm E}$ using Eq. (3). The upper limit of

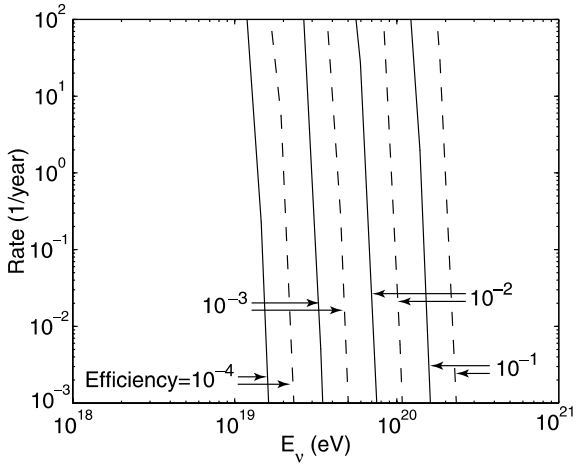

Fig. 10. False alarm rates λ for different detection efficiencies ε. The solid lines are for ν_e or $\bar{\nu}_e$ (producing an electromagnetic and an hadronic showers) while the dashed lines are for other neutrino flavors (where only the narrower beam from an hadronic shower is detected). The energy in abscissa is relative to the neutrino and it is shared between hadronic and leptonic components as expected for the energy of 10^{20} eV (20% hadronic and 80% leptonic).

the integration $V_{E,max}$ is determined from the condition that the acoustic radiation pattern is limited in size by the size of the detector, i.e. $R_E < R_{max}$, where $R_{max} \approx 100$ km. Finally, we get

$$\varepsilon = \frac{N_h}{V_w} \int_0^{V_{E,max}} p_{detect}(A, Y_{th})\, dV_E.$$

We can now use this expression to set the value of Y_{th} for any given efficiency ε and then calculate the resulting false alarm rate as $\lambda = N_h f_s p_{false}$, where p_{false} is determined from Y_{th} using Eq. (A.8). We plot the calculated false alarm rates for different efficiencies in Fig. 10a. The solid lines correspond to ν_e or $\bar{\nu}_e$ that produce electromagnetic and hadronic showers, while the dashed lines are for other neutrino flavors that produce a narrower sound lobe from the shorter hadronic shower. As expected, electromagnetic showers can afford a higher threshold that results in a lower false alarm rate.

5. Conclusions

We have reviewed the possibility of searching for ultra-high-energy neutrinos in cosmic rays using the acoustic emission from the electromagnetic and hadronic showers produced by the neutrino interactions in sea water. We have analyzed the expected statistical noise and devised an optimal algorithm to filter it out of the data stream in real-time. In a simulation we have applied this technique to trigger the data acquisition of a very large, high-frequency multi-hydrophone array of the US Navy and found that one could trigger on events at or above $\sim 10^{20}$ eV with tolerable false alarm rates. Our algorithms are based on signals from individual sensors, as appropriate for a trigger system, and are optimized to run on the array's digital signal processors. This would make a data taking campaign rather straightforward. Further off-line analysis would be needed to study the additional information that can be obtained by multi-hydrophone correlations. Although it is clear that an array with higher sensor density would allow lower energy thresholds and better redundancy, a test on the existent array analyzed here will provide information on coherent noise and give a definite assessment on the power of this technique.

Acknowledgements

We would like to thank D. Bryant, J. Cecil, N. DiMarzio, T. Kelly-Bissonnette, D. Moretti (US Navy) for the many discussions on the neutrino detection capabilities of AUTEC. We are also indebted to J. Vandenbroucke (Stanford) for the help in programming the AUTEC signal processors. One of us (G.G.) is indebted to D. Kapolka (US Navy) for early guidance in understanding the high frequency capabilities of different arrays. We thank P. Gorham (JPL) for a critical reading of an early version of the manuscript. This work was supported, in part, by a Terman Fellowship from the Stanford University. Partial support was also provided by the Office of Naval Research under grant no. N00014-93-1-0054.

Appendix A. The detection algorithm

In order to analyze the problem of signal detection in some detail we assume a discretized data

sample from a single hydrophone. Since the amplitude of the signal can vary with respect to the distance to the source, we only fix the *shape* of the signal, without specifying its amplitude in advance. Let us assume that the signal shape after discretization with sampling frequency f_s, is represented as an array of N real numbers, F_n, where $n = 0,\ldots,N-1$, so that the signal is AF_n, where A is the amplitude.

The discrete data sample x_k, $k = 0,\ldots,M-1$, which is discretized with sampling frequency f_s, is the sum of the stationary Gaussian noise w_k of a given power spectrum and a signal embedded at a random position $k_0 = 0,\ldots,M-N$ with an unknown amplitude A:

$$x_k = \begin{cases} w_k, & k < k_0 \text{ or } k \geqslant k_0 + N \\ w_k + AF_{k-k_0}, & k_0 \leqslant k < k_0 + N. \end{cases}$$

We will search for the signal position k_0 and the amplitude A which maximizes the conditional probability of a signal to be present within a given data set. This is a regression problem that can be solved by finding the maximum in the appropriate likelihood function [56]. Let us take a sub-sample of the original data $X_k \equiv x_{k_0+k}$, where $k = 0,\ldots,N-1$, and analogously define a noise sub-sample $W_k \equiv w_{k_0+k}$. The likelihood of the signal presence at position k_0 is given by the Bayes formula

$$\begin{aligned}&\mathrm{Prob}\{F, A \in [A, A+\mathrm{d}A]|X\} \\ &\quad = \frac{\mathrm{Prob}\{X|F,A\}\,\mathrm{Prob}\{F\} f(A)\,\mathrm{d}A}{\mathrm{Prob}\{X\}}. \end{aligned} \tag{A.1}$$

The ratio to the probability of the absence of signal (which is found in a similar manner) is

$$\begin{aligned}&\frac{\mathrm{Prob}\{F, A \in [A, A+\mathrm{d}A]|X\}}{\mathrm{Prob}\{\text{no signal}|X\}} \\ &\quad = \frac{\mathrm{Prob}\{X|F,A\}\mathrm{Prob}\{F\} f(A)\,\mathrm{d}A}{\mathrm{Prob}\{X|\text{no signal}\}\,\mathrm{Prob}\{\text{no signal}\}}. \end{aligned}$$

We notice that some of these conditional probabilities are related to the distribution of the Gaussian noise:

$$\begin{aligned}\mathrm{Prob}\{X|F,A\} &= f_W(X - AF)\,\mathrm{d}X, \\ \mathrm{Prob}\{X|\text{no signal}\} &= f_W(X)\,\mathrm{d}X, \end{aligned}$$

where $\mathrm{d}X = \prod_k \mathrm{d}X_k$. The probability distribution $f_W(W)$ of the Gaussian noise, defined so that $f_W(W)\,\mathrm{d}W$ is the probability that the noise values W_k are in the interval $\mathrm{d}W = \prod_{k=0}^{N-1} \mathrm{d}W_k$, is given by

$$f_W(W) = C \exp\left(-\frac{1}{2} W^T K^{-1} W \right),$$

where K is the noise covariance matrix defined as $K_{jk} = \langle W_j W_k \rangle$ that, for stationary noise, has the property of being a function of the difference $(k-j)$ only. If this portion of the time series is long enough so that the noise values separated by $>N/2$ points are not correlated, we can assume circular stationarity $K_{jk} = R_{(k-j) \bmod N}$, where R is an array of length N.

The calculations are easiest in a basis in which the covariance matrix is diagonal. For a circularly stationary signal, this is the basis of Fourier components

$$\widetilde{W}_k = \sum_{n=0}^{N-1} W_n \exp\left(-\frac{2\pi i}{N} kn \right), \quad k = 0,\ldots,N-1. \tag{A.2}$$

The distribution of the noise Fourier components is defined so that $f_{\widetilde{W}}(\widetilde{W})\,\mathrm{d}\widetilde{W}$ is the probability of $\widetilde{W}$ to be in the interval $\mathrm{d}\widetilde{W} = \mathrm{d}\widetilde{W}_0 \times \mathrm{d}\widetilde{W}_{N/2} \prod_{k=1}^{N/2-1} \mathrm{d}[\mathrm{Re}\,\widetilde{W}_k]\,\mathrm{d}[\mathrm{Im}\,\widetilde{W}_k]$. Hence the probability distribution is given by

$$f_{\widetilde{W}}(\widetilde{W}) = \tilde{C} \exp\left(-\frac{1}{2} \sum_k |\widetilde{W}_k|^2 / S_k \right),$$

where S_k, $k = 0,\ldots,N-1$ is the noise spectrum defined as $\langle \widetilde{W}_k^* \widetilde{W}_l \rangle = \delta_{kl} S_k$. This is related to the covariance matrix as $S = N\tilde{R}$, with R defined above.

Substituting $f_{\widetilde{W}}(\widetilde{W})$ we get the ratio of the likelihoods

$$\begin{aligned}&\frac{\mathrm{Prob}\{F, A \in [A, A+\mathrm{d}A]|X\}}{\mathrm{Prob}\{\text{no signal}|X\}} \\ &\quad = \frac{\mathrm{Prob}\{F\}}{\mathrm{Prob}\{\text{no signal}\}} \exp(L')\,\mathrm{d}A, \end{aligned}$$

where the argument of the exponential function is

$$L' = -\frac{1}{2} \sum_k \frac{1}{S_k} (|\tilde{X}_k - A\tilde{F}_k|^2 - |\tilde{X}_k|^2) + \ln f(A).$$

Instead of maximizing the original probability, we maximize the log-likelihood L'.

Since A is always positive and $\ln f(A) \approx$ const. for $A > 0$, we choose the optimal amplitude estimate $\bar{A}$ which maximizes L':

$$\bar{A} = \max\left\{0, \frac{\sum_k \mathrm{Re}(\tilde{X}_k \tilde{F}_k^*)/S_k}{\sum_k |\tilde{F}_k|^2/S_k}\right\}.$$

Substituting this value into L', we form a random variable

$$L = -\frac{1}{2}\sum_k \frac{1}{S_k}(|\tilde{X}_k - \bar{A}\tilde{F}_k|^2 - |\tilde{X}_k|^2)$$
$$= L'(\bar{A}) + \text{const.}$$

Note that the maximization with respect to A can be generalized to other parameters of the signal. Let $F^{(m)}$ be different signal shapes from a set given by an index m. Then to get the maximum likelihood of the signal shape we choose the value of m_0 such that $L^{(m_0)} = \max\{L^{(m)}\}$ (note that const. $= \ln f(A)$ is the same for all m).

It turns out that the equation for L can be simplified in terms of the number of calculations required. Substituting into it the expression for $\bar{A}$, we derive

$$L = \begin{cases} \frac{Y^2}{2\sigma_Y^2}, & Y > 0, \\ 0, & Y \leqslant 0, \end{cases}$$

where $Y = \sum_k \mathrm{Re}(\tilde{X}_k \tilde{F}_k^*)/S_k$ and $\sigma_Y^2 = \sum_k |\tilde{F}_k|^2/S_k$ can be shown to be the variance of Y. Substituting the Fourier transform definition (A.2) for $\tilde{X}$, we finally obtain

$$Y = \sum_{l=0}^{N-1} X_l H_l, \tag{A.3}$$

where

$$H_l = \sum_k (\tilde{F}_k/S_k)\exp(2\pi i k l/N). \tag{A.4}$$

The variable Y is thus the result of applying a digital filter with response function H or transfer function $\tilde{H}_k = N\tilde{F}_k/S_k$. The amount of calculation can be reduced even further, due to a fact that the quantity of H_k that are significantly different from zero is $N^* < N$. The number N^* is estimated to be $\sim\tau_{\mathrm{sig}} f_{\mathrm{s}}$ because H_k has the time duration of the same order as the duration of the signal, τ_{sig}. This last fact is confirmed by a direct calculation. Thus, for typical values of $f_{\mathrm{s}} = 10^5$ Hz and $\tau_{\mathrm{sig}} \simeq 10^{-4}$ s, we have $N^* \sim 10$. The number of floating-point operations (flops) required is then $\sim 10^6$ per second, which is feasible on modern DSP processors capable of more that 50 Mflops/s.

Signal detection can then be implemented at every hydrophone utilizing the fact that Y has different distributions $f_{Y,A}(Y)$ in the cases presence ($A \neq 0$) and absence ($A = 0$) of a signal. We choose a threshold value Y_{th} and decide that the signal is present (absent) when $Y \geqslant Y_{\mathrm{th}}$ ($Y < Y_{\mathrm{th}}$). Since the distributions $f_{Y,A}(Y)$ for the cases of signal presence and absence in general overlap, there will be the possibility of false alarms and signal misses. The threshold value has then to be chosen in an appropriate manner.

We now estimate the probabilities of false alarms and misses for a certain threshold Y_{th} by estimating the probability distribution $f_{Y,A}(Y)$ of the variable Y in the presence of a signal of amplitude A (including the no-signal situation as a particular case $A = 0$). Since Y is a linear combination of Gaussian variables, the distribution sought is also Gaussian

$$f_{Y,A}(Y) = \frac{1}{\sqrt{2\pi}\sigma_Y}\exp(-(Y - A\sigma_Y^2)^2/(2\sigma_Y^2)). \tag{A.5}$$

The probability of missing a signal is then

$$p_{\mathrm{miss}} = \int_{-\infty}^{Y_{\mathrm{th}}} f_{Y,A}(Y)\,\mathrm{d}Y$$
$$= 1 - \frac{1}{2}\mathrm{erfc}\left(\frac{Y_{\mathrm{th}} - A\sigma_Y^2}{\sqrt{2}\sigma_Y}\right), \tag{A.6}$$

while the probability of the signal detection is

$$p_{\mathrm{detect}} = 1 - p_{\mathrm{miss}} = \int_{Y_{\mathrm{th}}}^{\infty} f_{Y,A}(Y)\,\mathrm{d}Y$$
$$= \frac{1}{2}\mathrm{erfc}\left(\frac{Y_{\mathrm{th}} - A\sigma_Y^2}{\sqrt{2}\sigma_Y}\right). \tag{A.7}$$

Finally, the false alarm probability is

$$p_{\text{false}} = \int_{Y_{\text{th}}}^{\infty} f_{Y,A=0}(Y)\,\mathrm{d}L = \frac{1}{2}\operatorname{erfc}\left(\frac{Y_{\text{th}}}{\sqrt{2}\sigma_Y}\right). \quad \text{(A.8)}$$

In the expressions above $\operatorname{erfc}(x) = 1 - \operatorname{erf}(x)$ is the complementary error function. The above expressions can be inverted to derive Y_{th} from p_{detect} and p_{false}:

$$Y_{\text{th}} = \begin{cases} A\sigma_Y^2 + \sqrt{2}\sigma_Y \operatorname{erf}^{-1}(1 - 2p_{\text{detect}}), \\ \sqrt{2}\sigma_Y \operatorname{erf}^{-1}(1 - 2p_{\text{false}}). \end{cases} \quad \text{(A.9)}$$

where $\operatorname{erf}^{-1}(x)$ is the inverse error function.

References

[1] A.A. Watson, Phys. Rep. 333–334 (2000) 309.
[2] A.V. Olinto, Phys. Rep. 333–334 (2000) 329.
[3] K. Greisen, Phys. Rev. Lett. 16 (1966) 748.
[4] G.T. Zatsepin, V.A. Kuzmin, Sov. Phys. JETP Lett. 4 (1966) 78.
[5] F. Halzen, Phys. Rep. 333–334 (2000) 349.
[6] M. Vietri, Phys. Rev. Lett. 80 (1998) 3690.
[7] E. Waxman, Phys. Rev. Lett. 75 (1995) 386.
[8] E. Waxman, J. Bahcall, Phys. Rev. Lett. 78 (1997) 2292.
[9] T.K. Gaisser, F. Halzen, T. Stanev, Phys. Rep. 258 (1995) 173.
[10] R. Protheroe, in: D.T. Vickamasinghe, G.V. Bicknell, L. Ferrario (Eds.), Accretion Phenomena and Related Outflows, IAU Colloq. 163, Astronomical Society of the Pacific, San Francisco, 1997, p. 585.
[11] R. Protheroe, in: M. Shapiro, R. Silberberg, J. Wefel (Eds.), Towards the Millennium in Astrophysics: Problems and Prospects, World Scientific, Singapore, 1998, p. 149.
[12] R. Protheroe, High energy neutrino astrophysics, invited talk at Neutrino 98, Takayama, ADP-AT-98-8, astro-ph/9809144, 1998.
[13] K. Mannheim, Astropart. Phys. 3 (1995) 295.
[14] F.W. Stecker, M.H. Salamon, Space Sci. Rev. 75 (1996) 341.
[15] G. Domokos, B. Elliott, S. Kovesi-Domokos, J. Phys. G: Nucl. Part. Phys. 19 (1993) 899.
[16] S. Yoshida, M. Teshima, Prog. Theor. Phys. 89 (1993) 833.
[17] G. Sigl, S.J. Lee, D.N. Schramm, P. Coppi, Phys. Lett. B 392 (1997) 129.
[18] G. Sigl, S. Lee, P. Bhattacharjee, S. Yoshida, Phys. Rev. D 59 (1999) 043504.
[19] R. Gandhi, C. Quigg, M.H. Reno, I. Sarcevic, Astropart. Phys. 5 (1996) 81.
[20] T. O'Halloran, P. Sokolsky, S. Yoshida, Phys. Today 51 (1) (1998) 31.
[21] T.C. Weekes, Space Sci. Rev. 75 (1996) 1.
[22] P.W. Gorham, K.M. Liewer, C.J. Naudet, in: D. Kieda, M. Salaman, B. Dingus (Eds.). 26 Int. Cosmic Ray Conf., vol. 2, Contributed Papers, University of Utah, Salt Lake City, 1999, p. 479 (HE.6.3.15, http://krusty.physics.utah.edu/~icrc 1999/proceedings.html).
[23] P.W. Gorham, Astropart. Phys. 15 (2001) 177.
[24] J.G. Learned, Lunar neutrino physics, Tech. Rep. HDC-9-89, University of Hawaii at Manoa, 1989.
[25] G.A. Askarjan, Sov. J. At. Energy 3 (1957) 921.
[26] J.G. Learned, Phys. Rev. D 19 (1979) 3293.
[27] H. Bradner, ed., DUMAND – Deep Underwater Muon and Neutrino Detection: Proc. La Jolla workshop on acoustic detection of neutrinos, Institute of Geophysics and Planetary Physics, Scripps Institution of Oceanography, University of California, San Diego, 1977.
[28] A. Parvulesku, G.D. Curtis, in: W. Lauterborn (Ed.), Cavitation and Inhomogeneities in Underwater Acoustics, Springer, New York, 1980, p. 237.
[29] A. Roberts, Rev. Mod. Phys. 64 (1992) 259.
[30] L. Sulak, T. Armstrong, H. Baranger, M. Bregman, M. Levi, D. Mael, J. Strait, T. Bowen, A.E. Pifer, P.A. Polakos, et al., Nucl. Inst. Meth. 161 (1979) 203.
[31] J. Kwiecinski, A.D. Martin, A.M. Stasto, Phys. Rev. D 59 (1999) 093002.
[32] F.H. Fisher, V.P. Simmons, J. Acoust. Soc. Am. 62 (1977) 558.
[33] U.S. Navy, Atlantic undersea test and evaluation center range manual, 1994.
[34] K. Mitsui, Phys. Rev. D 45 (1992) 3051.
[35] R.E. Bolz, G.L. Tuve (Eds.), Handbook of tables for applied engineering science, second ed., CRC Press, Cleveland, 1973, p. 660.
[36] S.D. Hunter, W.V. Jones, D.J. Malbrough, A.L.V. Buren, A. Liboff, T. Bowen, J.J. Jones, J.G. Learned, H. Bradner, L. Pfeffer, et al., J. Acoust. Soc. Am. 69 (1981) 1557.
[37] L.M. Lyamshev, Sov. Phys. Usp. 35 (1992) 276.
[38] J. Alvarez-Muñiz, E. Zas, Phys. Lett. B 434 (1998) 396.
[39] L. Landau, I. Pomeranchuk, Dokl. Akad. Nauk SSSR 92 (1952) 735.
[40] L. Landau, I. Pomeranchuk, Dokl. Akad. Nauk SSSR 92 (1953) 535.
[41] A. Migdal, Phys. Rev. 103 (1956) 1811.
[42] A. Migdal, Sov. Phys. JETP 5 (1957) 527.
[43] P. Sokolsky. Introduction to Ultrahigh Energy Cosmic Ray Physics, Addison-Wesley, Redwood City, 1989, p. 29.
[44] J. Alvarez-Muñiz, E. Zas, Phys. Lett. B 411 (1997) 218.
[45] G.V. Domogatsky, Nucl. Phys. Proc. Suppl. 91 (2000) 438.
[46] A. Butkevich, L.G. Dedenko, S.K. Karaevsky, A.A. Mironovich, A.L. Provorov, I.M. Zheleznykh, Phys. Part. Nuclei 29 (1998) 266.
[47] J.T. Richelson, Sci. Am. 278 (2) (1998) 48.
[48] Atlantic Undersea Test and Evaluation Center, AUTEC home page (2000), http://www.npt.nuwc.navy.mil/autec.
[49] G.M. Wenz, J. Acoust. Soc. Am. 34 (1962) 1936.
[50] V.O. Knudsen, R.S. Alford, J.W. Emling, J. Marine Res. 7 (1948) 410.
[51] R.J. Urick, Principles of Underwater Sound, McGraw-Hill, New York, 1975, p. 189.
[52] C.L. Epifanio, Ph.D. Thesis, Scripps Institution of Oceanography, UCSD, 1997.

[53] P. Beckmann, A. Spizzichino, The Scattering of Electromagnatic Waves from Rough Surfaces, Macmillan, New York, 1963.
[54] P.A. Crowther, in: W. Lauterborn (Ed.), Cavitation and Inhomogeneities in Underwater Acoustics, Springer, New York, 1980, p. 194.
[55] V. Cappellini, A.G. Constantinides, P. Emiliani, Digital Filters and their Applications, Academic Press, New York, 1978, p. 267.
[56] R.V. Hogg, A.T. Craig, Introduction to Mathematical Statistics, fifth ed., Prentice-Hall, Englewood Cliffs, NJ, 1995, p. 471.